High-photovoltage all-polymer solar cells based on a diketopyrrolopyrrole-isoindigo acceptor polymer

High Photovoltage All-Polymer Solar Cells based on a Diketopyrrolopyrrole-Isoindigo Acceptor Polymer

Zhaojun Li,[a] Xiaofeng Xu,*[a] Wei Zhang,[b] Zewdneh Genene,[c] Wendimagegn Mammo,[c] Arkady Yartsev,[b] Mats R. Andersson,[d] René A. J. Janssen,*[e] and Ergang Wang*[a]

[a] Department of Chemistry and Chemical Engineering, Chalmers University of Technology, SE-412 96 Göteborg, Sweden

[b] Division of Chemical Physics, Lund University, Box 124, 221 00 Lund, Sweden

[c] Department of Chemistry, Addis Ababa University, P.O. Box 33658, Addis Ababa, Ethiopia

[d] Future Industries Institute, University of South Australia, Mawson Lakes Boulevard, Mawson Lakes SA 5095, Australia

[e] Molecular Materials and Nanosystems and Institute for Complex Molecular Systems, Eindhoven University of Technology, PO BOX 513, 5600 MB Eindhoven, The Netherlands

In this work, we synthesized and characterized two new *n*-type polymers PTDPP-PyDPP and PIID-PyDPP. The former polymer is composed of pyridine-flanked diketopyrrolopyrrole (PyDPP) and thiophene-flanked diketopyrrolopyrrole (TDPP). The latter polymer consists of PyDPP and isoindigo (IID). PIID-PyDPP exhibits a much higher absorption coefficient compared to the widely used naphthalene diimide (NDI)-based acceptor polymers, and its high-lying LUMO level affords it to achieve a high open-circuit voltage (V_{oc}). As a result, the all-polymer solar cell (all-PSC) fabricated from a high band gap polymer PBDTTS-FTAZ as donor and PIID-PyDPP as acceptor attained a high V_{oc} of 1.07 V with a power conversion efficiency (PCE) of 4.2%. So far, it is one of the highest PCEs recorded from all-PSCs using diketopyrrolopyrrole (DPP)-based acceptors. Gratifyingly, no obvious PCE decay was

observed in two weeks, unraveling good stability of the all-PSC. This work demonstrates that the electron-withdrawing PyDPP unit can be a promising building block for new acceptor polymers in all-PSCs.

Introduction

The research and development of high-performance polymer solar cells (PSCs) have intensified in recent years and power conversion efficiencies (PCEs) of single junction PSCs, using fullerene derivatives (e.g. PCBM) as acceptors, have exceeded 11%.[1] However, fullerene derivatives are thought to be non-ideal acceptors with some intrinsic drawbacks such as high cost, weak light absorption and low stability.[2,3] Therefore, all-polymer solar cells (all-PSCs), using conjugated polymers as both electron donors (D) and acceptors (A), have drawn increasing attention because they can afford complimentary absorption, high absorption coefficients, and easily tunable energy levels to achieve high open-circuit voltage (V_{oc}).[4-6] Unlike the widely investigated donor polymers, so far, only a few acceptor polymers can afford decent performance in all-PSCs.[7-11] Up till now, the synthesis of acceptor polymers mainly focuses on the naphthalene diimide (NDI)[12-15] and perylene diimide (PDI) units.[16-18] However, like PCBM, the lowest unoccupied molecular orbital (LUMO) levels of NDI- and PDI-based acceptor polymers are normally quite low (*ca.* −4.0 eV), which limit the V_{oc} of the resulting all-PSCs.[16,19,20] In addition, the NDI-based polymers usually show low absorption coefficients, and our recent study revealed that the NDI-based all-PSCs have undesirable stabilities.[19] Therefore, it is crucial to develop new acceptor polymers with high-lying LUMO levels, high absorption coefficients and good stabilities to boost the performance of all-PSCs. Among the various electron-deficient units, the strong electron-withdrawing diketopyrrolopyrrole (DPP) and isoindigo (IID) units are often used to synthesize photoactive materials and organic field effect transistors (OFETs).[21-26] DPP- and IID-based polymers exhibit broad absorption up to ~1000 nm, high electron mobility approaching 16 $cm^2 V^{-1} s^{-1}$, and high PCEs up to 9% in PCBM-

based PSCs.[23,27-30] Although these polymers performed well as donors in PSCs, so far, there are very few successful examples of all-PSCs fabricated by using DPP- or IID-based accepter polymers.[8,31,32] Very recently, a thiazole-flanked diketopyrrolopyrrole (DPP2Tz) unit was successfully used as a building block for acceptor polymers and the maximal PCEs of the DPP2Tz-based all-PSCs can attain 3% (Scheme 1).[31]

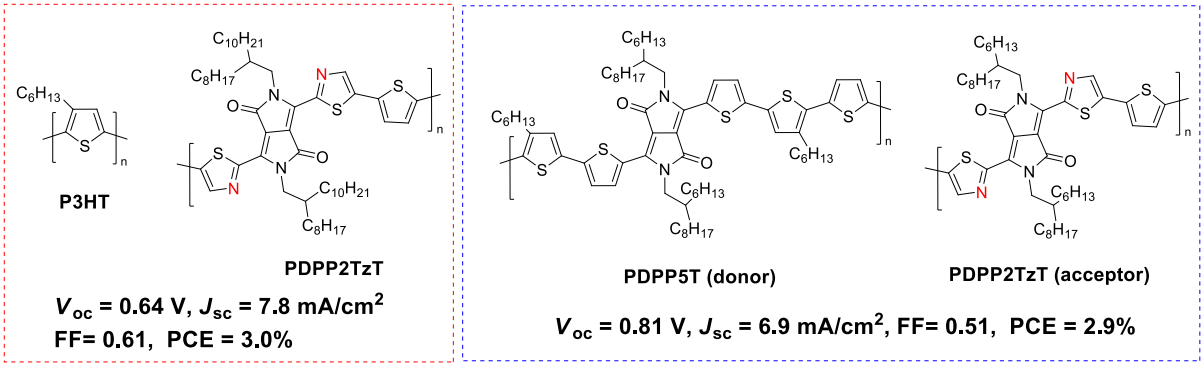

Scheme 1 DPP2Tz-based polymers for all-PSCs.

In our quest to synthesize desirable electron-deficient units for acceptor polymers, we notice that there is no report on the use of pyridine-flanked diketopyrrolopyrrole (PyDPP). A few early research indicated that the PyDPP unit can lower HOMO levels and provide wider band gap for the resulting polymers compared to the commonly used thiophene-flanked diketopyrrolopyrrole (TDPP) unit.[27,33,34] Inspired by the promising properties of the PyDPP unit, we synthesized two new PyDPP-based polymers PTDPP-PyDPP and PIID-PyDPP, incorporating the PyDPP unit with the TDPP and isoindigo (IID) units, respectively (Scheme 2). Compared to the NDI-based acceptor polymers and PCBM, PIID-PyDPP shows a higher absorption coefficient and a high-lying LUMO level. To investigate the photovoltaic performance of the two acceptor polymers in all-PSCs, we selected two donor polymers, a medium band gap polymer PTB7-Th and a high band gap polymer PBDTTS-FTAZ.[35,36] In this work, the PBDTTS-FTAZ:PIID-PyDPP all-PSC attains an encouraging PCE of 4.2%, which is one of the highest PCEs reported in all-PSCs using DPP-based acceptor polymers to date. The all-PSC features a high V_{oc} of 1.07 V as a consequence of the desired energy level alignment in

this D:A combination. In this work, the absorption properties, energy levels, charge transport mobilities, film morphology, exciton dissociation and bimolecular recombination are discussed and correlated to the photovoltaic performance of the PIID-PyDPP-based all-PSCs.

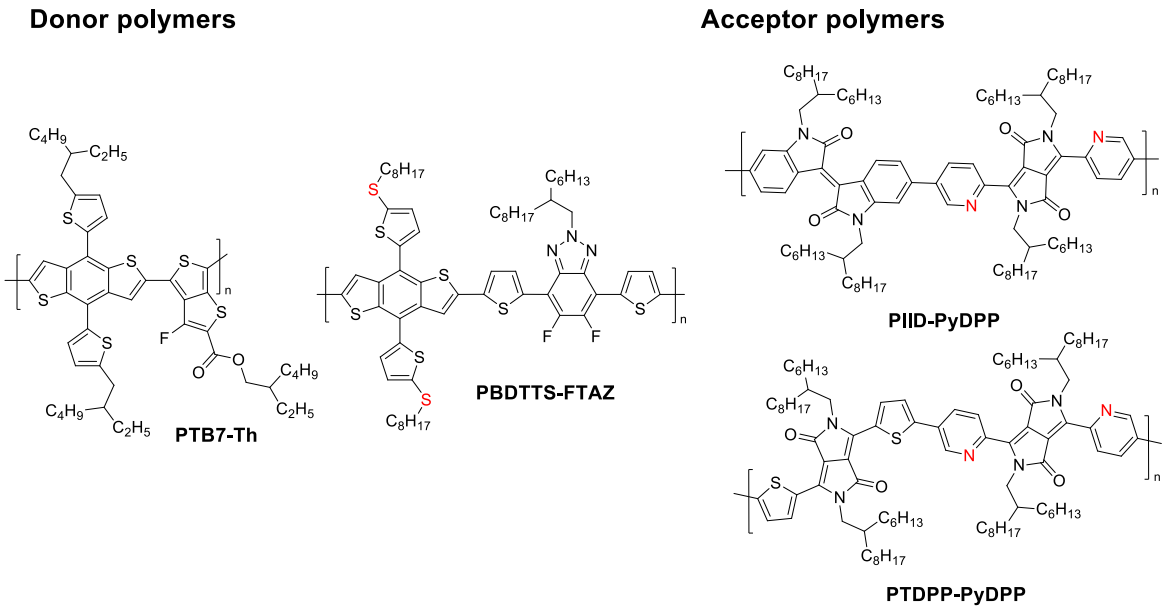

Scheme 2 Chemical structures of the donor and acceptor polymers.

Results and discussion

The synthetic routes of the dibromo-PyDPP monomer (**M1**) and diboronate ester monomer (**M2**) are depicted in Scheme S1 (ESI). **M1** was synthesized *via* a two-step reaction starting from 5-bromo-2-pyridinecarbonitrile (**1**).[27] The two acceptor polymers PTDPP-PyDPP and PIID-PyDPP were prepared via the Suzuki coupling polymerization of **M1** with **M2** and **M3**, respectively. (Scheme S2, ESI) The two polymers are readily soluble in common organic solvents, such as chloroform (CF), chlorobenzene (CB) and *o*-dichlorobenzene (*o*DCB) at room temperature. The molecular weights and polydispersity index (PDI) of the polymers were determined by gel permeation chromatography (GPC) at 150 °C, using 1,2,4-trichlorobenzene as the eluent. As summarized in Table 1, PTDPP-PyDPP and PIID-PyDPP show similar number-average molecular weights (M_n) of 23.1 kDa and 20.2 kDa, with PDI of 2.9 and 2.5, respectively.

Table1 Molecular weights and optical properties of donor and acceptor polymers

Polymer	M_n (kDa)	PDI	λ_{max} (nm)	E_g (eV)	ε_{sol} (L g^{-1} cm^{-1})	ε_{film} ($\times 10^4$ cm^{-1})
PTB7-Th	35.0	3.0	700	1.60	57.1	9.2
PBDTTS-FTAZ	22.6	3.2	600	1.90	56.9	11.3
PTDPP-PyDPP	23.1	2.9	792	1.43	32.3	5.5
PIID-PyDPP	20.2	2.5	667	1.69	42.1	8.1

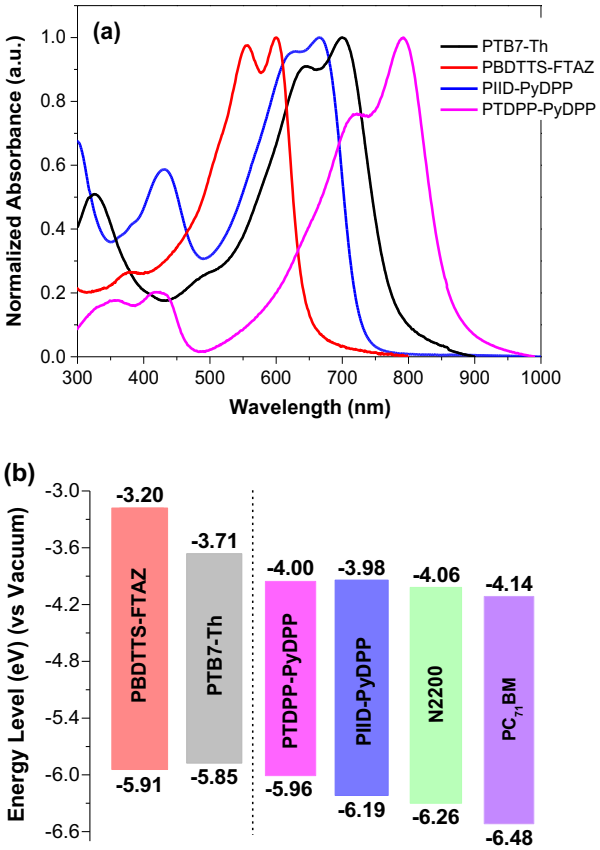

Fig. 1 (a) Normalized UV-vis-NIR absorption spectra of the polymers in thin films. (b) Energy level diagram of the polymers and $PC_{71}BM$.

As shown in Fig. 1 and Fig. S1a (ESI), all the polymers exhibit red-shifted and broader absorption spectra in thin films as compared to those in solution, due to the π-π stacking and/or intermolecular interactions in the solid state.[36] Thin films of PIID-PyDPP and PTDPP-PyDPP exhibit partly complementary absorption to the two donor polymers and thus better coverage

of the solar irradiation could be expected in the blend films (Fig. S1d, ESI). To evaluate the absorption capacities of the polymers, the absorption coefficients of the four polymers in solution and thin films were measured and depicted in Fig. S1b, Fig. S1c (ESI) and Table 1. The absorption coefficients of the two acceptor polymers are lower than those of the donor polymers, indicating that less contribution to light harvest stems from the acceptor polymers. It is worth noting that the absorption coefficient of PIID-PyDPP (8.1×10^4 cm^{-1}) is higher than those of NDI-based acceptor polymers ($3\times10^4 - 4\times10^4$ cm^{-1}) reported in the literature.[20,37-40]

The energy levels of the donor and acceptor materials are vital for the determination of V_{oc}, since V_{oc} is proportional to the energy offset between the HOMO of the donor and the LUMO of the acceptor.[41] In this work, the energy levels of the polymers and $PC_{71}BM$ were measured together by the square wave voltammetry (SWV). The HOMO and LUMO levels were calculated from the oxidation and reduction peak potentials (Fig. S2, ESI). As shown in Fig. 1b, the LUMO levels of the two acceptor polymers are up-shifted compared to N2200 and $PC_{71}BM$, thus a higher V_{oc} can be expected from the all-PSCs based on PIID-PyDPP and PTDPP-PyDPP. To ensure enough driving force for charge generation, the HOMO offset between the donor and acceptor, and the LUMO offset between the donor and acceptor are believed to be at least 0.3 eV.[42,43] The LUMO levels of PIID-PyDPP and PTDPP-PyDPP fulfill this criterion with respect to the LUMO levels of the two donor polymers PBDTTS-FTAZ and PTB7-Th, but not with respect to $PC_{71}BM$, signifying that PIID-PyDPP and PTDPP-PyDPP are unlikely to act as donors in combination with $PC_{71}BM$. Furthermore, the HOMO level of PTDPP-PyDPP is very close to those of the two donor polymers, suggesting that insufficient driving force may exist in the PTB7-Th:PTDPP-PyDPP and PBDTTS-FTAZ:PTDPP-PyDPP blends. The poor photovoltaic performance of the PTB7-Th:PTDPP-PyDPP all-PSCs discussed in the next section may be attributed to the insufficient driving force for charge separation.

Table 2 Photovoltaic parameters of the optimized PTB7-Th:PIID-PyDPP and PBDTTS-FTAZ:PIID-PyDPP all-PSCs[a]

donor:acceptor	V_{oc} (V)	J_{sc} (mA/cm^2)	FF	PCE (%)	SCLC μ_h (cm^2 V^{-1} s^{-1})	SCLC μ_e (cm^2 V^{-1} s^{-1})
PTB7-Th: PIID-PyDPP	1.02	5.9(6.1)[b]	0.39	2.3(2.2±0.1)[c]	2.4×10^{-4}	4.4×10^{-5}
PBDTTS-FTAZ: PIID-PyDPP	1.07	9.1(9.4)	0.43	4.2(4.1±0.1)[c]	7.1×10^{-5}	3.7×10^{-5}

[a] the optimized D:A ratio is 2.5:1 (w:w) and the optimized film thickness is around 85 nm. [b] the photocurrents obtained by integrating the EQE with the AM 1.5G spectrum are given in parentheses. [c] average PCEs of five devices are given in parentheses.

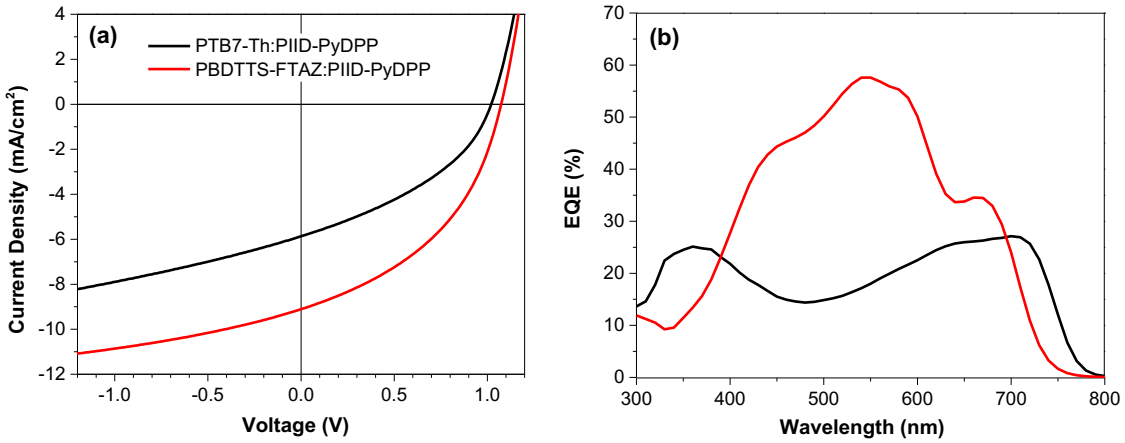

Fig. 2 (a) *J*–*V* curves of the optimized PTB7-Th:PIID-PyDPP (2.5:1 w:w) and PBDTTS-FTAZ:PIID-PyDPP (2.5:1 w:w) all-PSCs. (b) Corresponding EQE profiles of the all-PSCs.

PSCs were fabricated using an inverted configuration of ITO/ZnO/active layer/MoO_3/Ag. The active layer was processed from CB solution without any solvent additive or thermal treatment. The D:A ratios and the thicknesses of the active layers were optimized (Table S1, ESI). As summarized in Table S1a and S1b (ESI), the low performance of the two PSCs fabricated from PTDPP-PyDPP:$PC_{71}BM$ and PIID-PyDPP:$PC_{71}BM$ may be ascribed to the very small LUMO-LUMO offsets in these systems and thus cannot provide enough driving force for exciton dissociation. Likewise, the PTB7-Th:PTDPP-PyDPP all-PSC also shows a very low PCE of 0.02%, consistent with the small HOMO-HOMO offset. Assuming that there is a similar trend in the photovoltaic performance, we refrained from fabricating the PBDTTS-

FTAZ:PTDPP-PyDPP all-PSC in this work. In contrast, the PTB7-Th:PIID-PyDPP and PBDTTS-FTAZ:PIID-PyDPP blends can afford efficient all-PSCs due to their sufficient LUMO-LUMO and HOMO-HOMO offsets (Table 2 and Fig. 2a). The PTB7-Th:PIID-PyDPP all-PSC shows a V_{oc} of 1.02 V, which is higher than the reported values for the PTB7-Th:PCBM (~0.83 V) and PTB7-Th:N2200 (~0.80 V) PSCs.[20,35,37] It is consistent with the higher-lying LUMO level of PIID-PyDPP compared to $PC_{71}BM$ and N2200. However, the low fill factor (FF) of 0.39 and short-circuit current density (J_{sc}) of 5.9 mA/cm^2 lead to a moderate PCE of 2.3% in this all-PSC. The PBDTTS-FTAZ:PIID-PyDPP all-PSC attains a higher V_{oc} of 1.07 V, which presumably originates from the high-lying LUMO level of PIID-PyDPP and the low-lying HOMO level of PBDTTS-FTAZ.[36] Combined with a J_{sc} of 9.1 mA/cm^2 and a moderate FF of 0.43, an improved PCE of 4.2% was achieved, which is among the highest PCEs in all-PSCs fabricated with DPP-based polymers as acceptors. Interestingly, the highest PCEs of the two all-PSCs were recorded when a donor-rich D:A ratio (2.5:1 w/w) was used, which is different from other reports on the PTB7-Th-based all-PSCs, where the best performances were achieved when equivalent amounts of D and A (1:1 w/w) were used.[10,35,37]

The external quantum efficiency (EQE) was measured to evaluate the spectral responses and the accuracies of the photocurrents in *J*–*V* measurements. For both the PTB7-Th:PIID-PyDPP and PBDTTS-FTAZ:PIID-PyDPP all-PSCs, the photoresponse of the EQE curves are consistent with the absorption spectra of the blend films, which corroborates the photocurrent contribution from both the donor and acceptor polymers (Fig. 2b and Fig. S1d, ESI). The EQE of the PBDTTS-FTAZ:PIID-PyDPP all-PSC exceeds 50% in the range of 550–600 nm, and reaches 34% at around 667 nm, which clearly stems from the acceptor polymer. Considering that there is only 28% (feed ratio in weight) acceptor polymer in the blend, the EQE at around 667 nm is likely limited by insufficient light absorption. The calculated J_{sc} obtained by

integrating the EQE with the AM1.5G spectrum is in good agreement with the J_{sc} from the J–V curves with a mismatch of less than 4%.

In order to further understand the limits of the V_{oc} in the PBDTTS-FTAZ:PIID-PyDPP all-PSC, the energy loss (E_{loss}) of this all-PSC was calculated to be 0.62 eV by using the equation: $E_{loss} = E_g - eV_{oc}$, where E_g is the lowest optical gap of the donor and acceptor. The minimal E_{loss} of PSCs is suggested to be 0.6 eV.[44] Although in practice many PSCs have an E_{loss} that is much higher than this threshold, very recent reports on new donor materials show that PCBM-based PSCs can feature high V_{oc} and low E_{loss} (< 0.6 eV) at the same time.[10,45-47] Here, to gain a better insight of the E_{loss} in all-PSCs, we summarized the E_{loss}, E_g and maximum EQE (EQE_{max}) of all-PSCs with PCEs over 2% (Table S2, ESI). Fig. S3a (ESI) depicts the plot of eV_{oc} against E_g. The E_{loss} of the PBDTTS-FTAZ:PIID-PyDPP all-PSC (0.62 eV) approaches the empirical threshold of E_{loss} (0.6 eV). This indicates that the V_{oc} of 1.07 V obtained for this cell is close to the practical limit that can be expected for an E_g of 1.69 eV. The plot of EQE_{max} against E_{loss} is shown in Fig. S3b (ESI). The EQE_{max} of the PBDTTS-FTAZ:PIID-PyDPP all-PSC is in fact among the highest values reported in all-PSCs when the E_{loss} is close to 0.60 eV, suggesting a low E_{loss} and high EQE can be realized at the same time in all-PSCs.

The charge transport properties of the polymer:polymer blends were evaluated by space charge limited current (SCLC) measurements. The J–V and SCLC fitting curves are shown in Fig. S4 (ESI). In both blends, the hole mobility (μ_h) and electron mobility (μ_e) are fairly balanced such that space charge effects are unlikely to play an important role.[48] We surmise that the relatively low FF may attribute to the unbalanced excitons dissociation efficiencies of the donor and acceptor polymers, which is also correlated to the non-ideal D/A morphology.[49] In such case, the photocurrent density only slowly saturates under reverse bias because the enhanced electric field promotes charge separation, which can be seen in Fig. 2a.

To further quantify the bimolecular recombination losses of the all-PSCs, we measured the EQE response with bias light illumination at wavelength of 530 nm. Since the bimolecular recombination strongly depends on the charge carrier density, the extra bias illumination increases the charge carrier density and lead to more realistic EQE profiles of the all-PSCs in the short-circuit condition.[50] The ratio of the EQEs measured with and without bias light (EQE_{nobias}/EQE_{bias}) can quantitatively characterize the bimolecular recombination, which is believed to be a more precise way in comparison with simply measuring the J_{sc} as a function of light intensity.[50,51] The bimolecular recombination efficiency (η_{BR}) can be approximated by $\eta_{BR} = EQE_{nobias}/EQE_{bias} - 1$, where a lower η_{BR} suggests less bimolecular recombination.[50,51] As shown in Fig. S5 (ESI), the PBDTTS-FTAZ:PIID-PyDPP all-PSC exhibits a relatively low η_{BR} around 0.08, suggesting that separated charges can be efficiently transported and collected by the electrodes. On the other hand, the PTB7-Th:PIID-PyDPP all-PSC represents significant bimolecular recombination with a much higher η_{BR} around 0.18. This result suggests that the bimolecular recombination is one of the main losses in the PTB7-Th:PIID-PyDPP all-PSC, which leads to the reduction of J_{sc}.

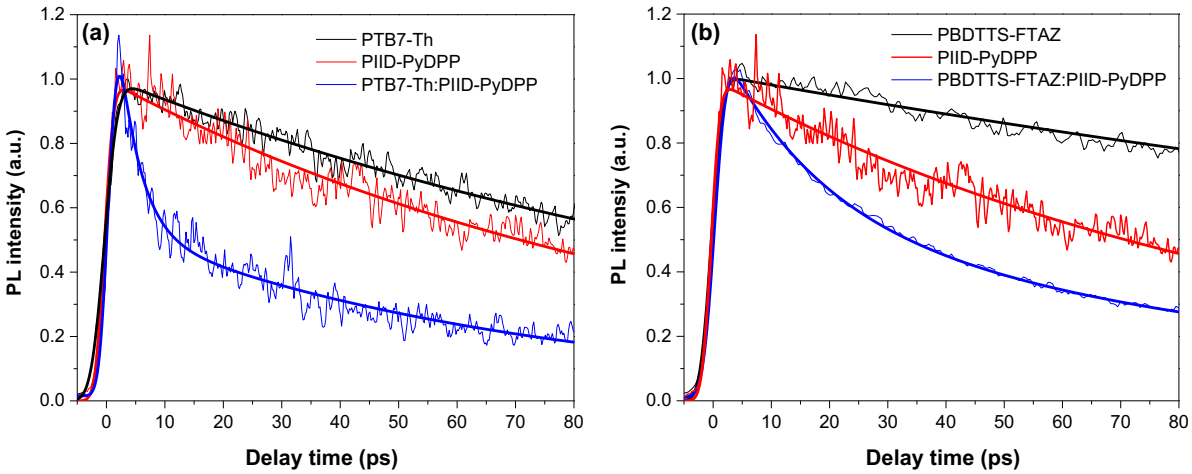

Fig. 3 kinetic traces of the neat and blend films.

To gain insight into the exciton diffusion and dissociation processes in the blend films, we conducted time-resolved photoluminescence (TRPL) measurements. Samples were excited at

400 nm and TRPL kinetics were obtained at 810 and 750 nm for PTB7-Th:PIID-PyDPP and PBDTTS-FTAZ:PIID-PyDPP blend films, respectively. The normalized TRPL traces are shown in Fig. 3 and lifetimes (τ) and are summarized in Table S3 (ESI). We find that the TRPL of each blend decays faster than those of the corresponding neat donor or acceptor films. In the blends, the TRPL follows a bi-exponential decay, reflecting that not all primary excitations are equally effectively quenched. To estimate the overall exciton quenching efficiencies of the individual polymers in the blend films, we first measured the absolute fluorescence quantum yields (Φ) of the neat polymers and blend films, which directly reflects the efficiency of the conversion of absorbed photons into emitted photons. An integrating sphere setup was used to collect all the emission from the samples, allowing the determination of absolute quantum yields without the need for a quantum yield standard. An intense laser with an excitation wavelength of 532 nm was used. In this work, we found that the PL spectra of the donor and acceptor polymers are mostly overlapped and a much weaker Φ is obtained from the acceptor polymer, thus it is difficult to distinguish the individual contributions of the donor and acceptor to the quantum yields of the blend films (Table S4, ESI). In this case, if we assume that the quantum yield of the blend only stems from the donor, the calculated exciton quenching efficiencies (η) of PTB7-Th and PBDTTS-FTAZ in the blend films are 70% and 91% (Table S4, ESI), respectively, which can be an indication of the minimal η in each blend. Because the acceptor somewhat contributes to the quantum yield of the blend film, in an actual case, the quenching efficiency of the donor should be higher than the value we obtained above. Therefore, it demonstrates that, at least, the generated excitons in the two donor polymers can dissociate efficiently in the blend films.

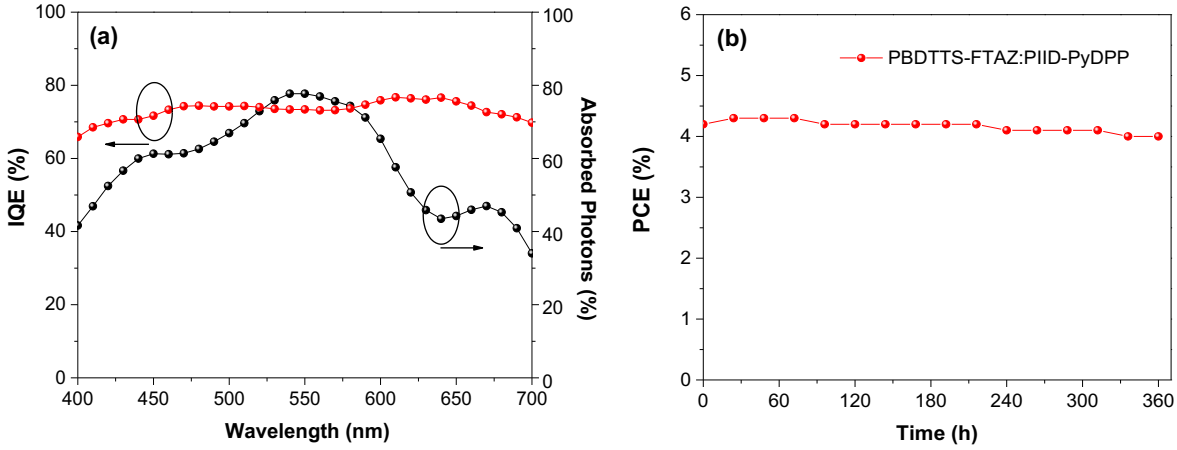

Fig. 4 (a) IQE curve of the PBDTTS-FTAZ:PIID-PyDPP all-PSCs and absorbed photons of the PBDTTS-FTAZ:PIID-PyDPP (2.5:1 w:w) blend (b) Stability test of the PBDTTS-FTAZ:PIID-PyDPP (2.5:1 w:w) all-PSCs.

Since the PBDTTS-FTAZ:PIID-PyDPP all-PSC shows a high EQE, it would be of interest to evaluate the efficiency of collected carriers per absorbed photon. Therefore, we determined the internal quantum efficiency (IQE) from the corresponding EQE and the total fraction of absorbed photons. The absorbed photon spectrum was simulated from the wavelength-dependent refractive index (n) and extinction coefficient (k) of all the layers via optical modelling of the entire layer stack (Fig. S6, ESI). As shown in Fig. 4a, the IQE stays above 70% from 450 to 700 nm. The bias-dependent photocurrent (Fig. 2a) indicates that possibly even a larger fraction than 70% of the absorbed photons in the PBDTTS-FTAZ:PIID-PyDPP blend is converted into charge carriers at the D/A interface. In this case, the higher exciton quenching efficiency inferred from the absolute fluorescence quantum yield is in reasonable agreement with the IQE value.

Although good stability is essential for the practical application of PSCs, there are very few reports on the stability study of all-PSCs.[19] In general, inverted PSCs are inherently more stable compared to conventional PSCs, due to the absence of the poly(3,4-ethylenedioxythiophene)-poly(styrenesulfonate) (PEDOT:PSS) layer and the use of low work function anodes.[52,53] Here, we studied the stabilities of the inverted PBDTTS-FTAZ:PIID-PyDPP all-PSCs, by measuring

their PCEs every 24 hours at room temperature in glove box. No obvious reduction in PCEs is observed in these all-PSCs and PCEs retain more than 90% of the initial value after two weeks (Fig. 4b). The preliminary stability study of this all-PSC is contrary to our previous observation from the TQ1:N2200 all-PSCs, where the performance degraded very quickly.[19]

Conclusion

In summary, we developed two new acceptor polymers based on the PyDPP moiety with up-shifted LUMO levels compared to $PC_{71}BM$ with the intention of achieving higher V_{oc}. The low band gap and high-lying HOMO level of the polymer PTDPP-PyDPP make it unsuitable as an acceptor polymer. In contrast, the wider band gap polymer PIID-PyDPP, with its lower lying HOMO and enhanced absorption coefficient, is proved to be a suitable acceptor polymer in combination with either PTB7-Th or PBDTTS-FTAZ as donor. Compared to the PTB7-Th:PIID-PyDPP all-PSC, the PBDTTS-FTAZ:PIID-PyDPP all-PSC realizes a more complementary absorption spectrum and less bimolecular recombination, which attains an encouraging PCE of 4.2%, featuring a very high V_{oc} of 1.07 eV due to the low E_{loss} of 0.62 eV. So far, it is one of the best performance among the all-PSCs using DPP-based acceptor polymers, and also among the top performance reported from all-PSCs containing other than NDI-based acceptor polymers. This work demonstrates that the PyDPP unit can be a promising alternative to the widely used NDI unit for the synthesis of new acceptor polymers in high-performance and stable all-PSCs.

Experimental section

Material Characterization. GPC was performed on an Agilent PL-GPC 220 Integrated High Temperature GPC/SEC System equipped with refractive index and viscometer detectors at 150 °C working temperature. The columns were 3 PLgel 10 μm MIXED-B LS 300 × 7.5 mm columns and the eluent was 1,2,4-trichlorobenzene. The molecular weights of polymers were

calculated according to relative calibration with polystyrene standards. UV-vis-NIR absorption spectra of the two copolymers were measured with a Perkin Elmer Lambda 900 UV-vis-NIR absorption spectrometer and SWV measurements were carried out on a CH-Instruments 650A Electrochemical Workstation. A three-electrode setup was used with platinum wires for both working electrode and counter electrode, and Ag/Ag^+ was employed as the reference electrode calibrated with a ferrocene/ferrocenyl couple (Fc/Fc^+). The supporting electrolyte was a 0.1 M solution of tetrabutylammonium hexa-uorophosphate (Bu_4NPF_6) in anhydrous acetonitrile saturated with nitrogen. The polymer films were deposited onto the working electrode from chloroform solution.

Fabrication and Characterization of All-PSCs. Inverted all-PSC devices were fabricated on glass substrates, using an indium tin oxide (ITO)/ ZnO (40 nm)/ Active layer/ MoO_3 (10 nm)/ Ag (100 nm) structure. Sol-gel ZnO (thickness of around 40 nm, determined by a Dektak 6 M surface profilometer) was spin-coated onto the pre-cleaned ITO-coated glass substrate at a spinning rate of 4000 rpm for 60 s, followed by annealing at 150 °C for 5 mins. The active layer was then spin-coated on top of the ZnO layer in the glove box. All blended films used in this study were spin-coated from CB solutions in which the donor and acceptor polymers were dissolved with different weight ratios. The total concentration of these blended solutions was maintained at 12 mg/mL. After spin-coating, they were directly transferred to a vapour deposition system inside of the glove box. MoO_3 (10 nm) and Ag (100 nm), which were used as the top electrodes, were deposited via a mask under 3×10^{-4} Pa vacuum onto the active layer. The accurate area of every device (9 mm^2 or 16 mm^2), defined by the overlap of the ITO and metal electrode, was calibrated carefully by microscope. The *J–V* characteristics were recorded by a Keithley 2400 source meter under the illumination of an AM 1.5 G solar simulator with an intensity of 100 mW/cm^2 (a tungsten-halogen lamp filtered by a Hoya LB120 daylight filter.). The light intensity was determined by a standard silicon photodiode. EQE measurements were

performed in a homebuilt setup. All the devices were kept in a nitrogen-filled box with a quartz window, and illuminated through an aperture of 2 mm. A mechanical chopper (Stanford Research, SR 540) and a monochromator (Oriel, Cornerstone 130) were utilized to modulate the white light of a 50 W tungsten halogen lamp (Osram 64610). A 530 nm light power LED (Thorlabs) was used to illuminate the solar cell simultaneously under the mechanically modulated monochromatic light to carry out the EQE measurements under bias light. The differential photocurrent density was picked up by a lock-in amplifier and the current was recorded as the voltage over a 50 Ω resistance. It was converted to EQE profile by comparing the data with a silicon reference cell.

SCLC mobility measurement. Hole mobility was measured in a hole-only device composed of ITO/PEDOT:PSS (40 nm)/active layer/Au (100 nm). Electron mobility was measured in an electron-only device composed of ITO/ZnO (40 nm)/active layer/LiF (1 nm)/Al (100 nm). The mobility μ was calculated using the following equation:

$$J = \frac{9}{8}\varepsilon\varepsilon_0\mu\frac{(V-V_{bi})^2}{d^3}$$

TRPL measurement. A Ti:Sapphire laser (Spectra-Physics, Tsunami) at 800 nm was used as an excitation source with repetition rate of 80 MHz and pulse duration of 100 fs and a frequency-doubled light (400 nm, generated by Photop Technologies, Tripler TP-2000B) was used for excitation. Two 1-inch quartz plano-convex lenses of 50 mm focal length were used to collect PL and focused on the input slit of a spectrograph (Chromex). A streak camera (Hamamatsu C6860) with a slit width of 20 μm was used to collect the output of the spectrograph. Background correction of the measured PL images was performed first and then the shading and spectral sensitivity correction of the fluorescence spectrometer was carried out with calibrated reference light source (Ocean Optics, LS-1-CAL). All measurements were carried out at room temperature.

Absolute fluorescence quantum yield measurement. A CW laser (532 nm, excitation density 2.5 mJ/cm^2) was used to excite the samples placed inside an integrating sphere (HORIBA, Quanta-φ, F3029). The output light was guided into a monochromator with optical fibers, and the signal was recorded by a photomultiplier tube or a CCD detector.

Acknowledgements

We thank the EU projects OSNIRO (FP7-PEOPLE-2013-ITN, Grant agreement no.: 607585) and SUNFLOWER (FP7-ICT-2011-7, Grant number: 287594), the Swedish Research Council, the Swedish Research Council Formas, the Swedish Energy Agency and Chalmers Area of Advanced Energy for financial support. R. A. J. J acknowledges funding from the European Research Council under the European Union's Seventh Framework Programme (FP/2007-2013) / ERC Grant Agreement No. 339031 and the Ministry of Education, Culture, and Science (NWO Gravity program 024.001.035). W. Z and A. Y acknowledges the Knut and Alice Wallenberg and Crafoord foundations. W. M and Z. G acknowledge financial support from the International Science Programme (ISP), Uppsala University, Sweden. We thank Dario Di Carlo Rasi for the training on device fabrication and characterization. The research leading to these results has received funding from the People Programme (Marie Curie Actions) of the European Union's Seventh Framework Programme (FP7/2007-2013) under REA grant agreement n° 608743. This publication reflects only the view of the authors and the European Union is not liable for any use that may be made of the information contained herein. We thank Dr. Harm van Eersel using the python script to calculate the optical parameters in the IQE simulation.

Notes and references

1. J. Zhao, Y. Li, G. Yang, K. Jiang, H. Lin, H. Ade, W. Ma and H. Yan, *Nat. Energy*, 2016, **1**, 15027.
2. M. Granström, K. Petritsch, A. Arias, A. Lux, M. Andersson and R. Friend, *Nature*, 1998, **395**, 257-260.
3. I. H. Jung, W.-Y. Lo, J. Jang, W. Chen, D. Zhao, E. S. Landry, L. Lu, D. V. Talapin and L. Yu, *Chem. Mater.*, 2014, **26**, 3450-3459.
4. Y. Lin and X. Zhan, *Mater. Horiz.*, 2014, **1**, 470-488.

5. H. Benten, D. Mori, H. Ohkita and S. Ito, *J. Mater. Chem. A*, 2016, **4**, 5340-5365.
6. H. Kang, W. Lee, J. Oh, T. Kim, C. Lee and B. J. Kim, *Acc. Chem. Res.*, 2016, **49**, 2424-2434.
7. D. Mori, H. Benten, H. Ohkita, S. Ito and K. Miyake, *ACS Appl. Mater. Interfaces*, 2012, **4**, 3325-3329.
8. W. Li, Y. An, M. M. Wienk and R. A. Janssen, *J. Mater. Chem. A*, 2015, **3**, 6756-6760.
9. R. Zhao, C. Dou, Z. Xie, J. Liu and L. Wang, *Angew. Chem.*, 2016, **128**, 5399-5403.
10. X. Long, Z. Ding, C. Dou, J. Zhang, J. Liu and L. Wang, *Adv. Mater.*, 2016, **28**, 6504-6508.
11. M. A. Uddin, Y. Kim, R. Younts, W. Lee, B. Gautam, J. Choi, C. Wang, K. Gundogdu, B. J. Kim and H. Y. Woo, *Macromolecules*, 2016, **49**, 6374-6383.
12. T. Kim, J.-H. Kim, T. E. Kang, C. Lee, H. Kang, M. Shin, C. Wang, B. Ma, U. Jeong and T.-S. Kim, *Nat. Commun.*, 2015, **6**, 8547.
13. C. Lee, H. Kang, W. Lee, T. Kim, K. H. Kim, H. Y. Woo, C. Wang and B. J. Kim, *Adv. Mater.*, 2015, **27**, 2466-2471.
14. Y. J. Hwang, B. A. Courtright, A. S. Ferreira, S. H. Tolbert and S. A. Jenekhe, *Adv. Mater.*, 2015, **27**, 4578-4584.
15. L. Gao, Z. G. Zhang, L. Xue, J. Min, J. Zhang, Z. Wei and Y. Li, *Adv. Mater.*, 2016, **28**, 1884-1890.
16. S. Li, H. Zhang, W. Zhao, L. Ye, H. Yao, B. Yang, S. Zhang and J. Hou, *Adv. Energy Mater.*, 2015, **6**, 1501991.
17. Y.-J. Hwang, T. Earmme, B. A. Courtright, F. N. Eberle and S. A. Jenekhe, *J. Am. Chem. Soc.*, 2015, **137**, 4424-4434.
18. S. Nam, S. G. Hahm, H. Han, J. Seo, C. Kim, H. Kim, S. R. Marder, M. Ree and Y. Kim, *ACS Sustainable Chem. Eng.*, 2016, **4**, 767-774.
19. Y. Xia, C. Musumeci, J. Bergqvist, W. Ma, F. Gao, Z. Tang, S. Bai, Y. Jin, C. Zhu and R. Kroon, *J. Mater. Chem. A*, 2016, **4**, 3835-3843.
20. Z. Li, X. Xu, W. Zhang, X. Meng, W. Ma, A. Yartsev, O. Inganäs, M. R. Andersson, R. A. J. Janssen and E. Wang, *J. Am. Chem. Soc.*, 2016, **138**, 10935−10944.
21. X. Guo, A. Facchetti and T. J. Marks, *Chem. Rev.*, 2014, **114**, 8943-9021.
22. E. Wang, W. Mammo and M. R. Andersson, *Adv. Mater.*, 2014, **26**, 1801-1826.
23. W. Li, K. H. Hendriks, M. M. Wienk and R. A. Janssen, *Acc. Chem. Res.*, 2015, **49**, 78-85.
24. E. Wang, Z. Ma, Z. Zhang, K. Vandewal, P. Henriksson, O. Inganäs, F. Zhang and M. R. Andersson, *J. Am. Chem. Soc.*, 2011, **133**, 14244-14247.
25. Z. Ma, D. Dang, Z. Tang, D. Gedefaw, J. Bergqvist, W. Zhu, W. Mammo, M. R. Andersson, O. Inganäs, F. Zhang and E. Wang, *Adv. Energy Mater.*, 2014, **4**, n/a-n/a.
26. D. I. James, S. Wang, W. Ma, S. Hedström, X. Meng, P. Persson, S. Fabiano, X. Crispin, M. R. Andersson, M. Berggren and E. Wang, *Adv. Electron. Mater.*, 2016, **2**, 1500313.
27. B. Sun, W. Hong, Z. Yan, H. Aziz and Y. Li, *Adv. Mater.*, 2014, **26**, 2636-2642.
28. Y. Deng, J. Liu, J. Wang, L. Liu, W. Li, H. Tian, X. Zhang, Z. Xie, Y. Geng and F. Wang, *Adv. Mater.*, 2014, **26**, 471-476.
29. H. Choi, S. J. Ko, T. Kim, P. O. Morin, B. Walker, B. H. Lee, M. Leclerc, J. Y. Kim and A. J. Heeger, *Adv. Mater.*, 2015, **27**, 3318-3324.
30. Y. Lei, P. Deng, M. Lin, X. Zheng, F. Zhu and B. S. Ong, *Adv. Mater.*, 2016, **28**, 6687-6694.
31. W. Li, W. Roelofs, M. Turbiez, M. M. Wienk and R. A. Janssen, *Adv. Mater.*, 2014, **26**, 3304-3309.
32. F. Grenier, P. Berrouard, J.-R. Pouliot, H.-R. Tseng, A. J. Heeger and M. Leclerc, *Polym. Chem.*, 2013, **4**, 1836-1841.

33. J. W. Jung, F. Liu, T. P. Russell and W. H. Jo, *Chem. Commun.*, 2013, **49**, 8495-8497.
34. X. Zhang, C. Xiao, A. Zhang, F. Yang, H. Dong, Z. Wang, X. Zhan, W. Li and W. Hu, *Polym. Chem.*, 2015, **6**, 4775-4783.
35. S. H. Liao, H. J. Jhuo, Y. S. Cheng and S. A. Chen, *Adv. Mater.*, 2013, **25**, 4766-4771.
36. Z. Genene, J. Wang, X. Meng, W. Ma, X. Xu, R. Yang, W. Mammo and E. Wang, *Adv. Electron. Mater.*, 2016, 1600084.
37. D. Mori, H. Benten, I. Okada, H. Ohkita and S. Ito, *Energy Environ. Sci.*, 2014, **7**, 2939-2943.
38. J. Choi, K.-H. Kim, H. Yu, C. Lee, H. Kang, I. Song, Y. Kim, J. H. Oh and B. J. Kim, *Chem. Mater.*, 2015, **27**, 5230-5237.
39. K. D. Deshmukh, T. Qin, J. K. Gallaher, A. C. Liu, E. Gann, K. O'Donnell, L. Thomsen, J. M. Hodgkiss, S. E. Watkins and C. R. McNeill, *Energy Environ. Sci.*, 2015, **8**, 332-342.
40. H. Kang, M. A. Uddin, C. Lee, K.-H. Kim, T. L. Nguyen, W. Lee, Y. Li, C. Wang, H. Y. Woo and B. J. Kim, *J. Am. Chem. Soc.*, 2015, **137**, 2359-2365.
41. M. C. Scharber, D. Mühlbacher, M. Koppe, P. Denk, C. Waldauf, A. J. Heeger and C. J. Brabec, *Adv. Mater.*, 2006, **18**, 789-794.
42. A. J. Heeger, *Adv. Mater.*, 2014, **26**, 10-28.
43. G. Ren, C. W. Schlenker, E. Ahmed, S. Subramaniyan, S. Olthof, A. Kahn, D. S. Ginger and S. A. Jenekhe, *Adv. Funct. Mater.*, 2013, **23**, 1238-1249.
44. D. Veldman, S. C. Meskers and R. A. Janssen, *Adv. Funct. Mater.*, 2009, **19**, 1939-1948.
45. K. Kawashima, Y. Tamai, H. Ohkita, I. Osaka and K. Takimiya, *Nat. Commun.*, 2015, **6**, 10085.
46. Y. Li, X. Liu, F.-P. Wu, Y. Zhou, Z.-Q. Jiang, B. Song, Y. Xia, Z.-G. Zhang, F. Gao and O. Inganäs, *J. Mater. Chem. A*, 2016, **4**, 5890-5897.
47. C. Wang, X. Xu, W. Zhang, J. Bergqvist, Y. Xia, X. Meng, K. Bini, W. Ma, A. Yartsev, K. Vandewal, M. R. Andersson, O. Inganäs, M. Fahlman and E. Wang, *Adv. Energy Mater.*, 2016, **6**, 1600148.
48. C. M. Proctor, M. Kuik and T.-Q. Nguyen, *Prog. Polym. Sci.*, 2013, **38**, 1941-1960.
49. D. Veldman, Ö. İpek, S. C. J. Meskers, J. Sweelssen, M. M. Koetse, S. C. Veenstra, J. M. Kroon, S. S. v. Bavel, J. Loos and R. A. J. Janssen, *J. Am. Chem. Soc.*, 2008, **130**, 7721-7735.
50. L. Koster, M. Kemerink, M. M. Wienk, K. Maturová and R. A. Janssen, *Adv. Mater.*, 2011, **23**, 1670-1674.
51. D. J. Wehenkel, K. H. Hendriks, M. M. Wienk and R. A. Janssen, *Org. Electron.*, 2012, **13**, 3284-3290.
52. T. Yang, W. Cai, D. Qin, E. Wang, L. Lan, X. Gong, J. Peng and Y. Cao, *J. Phys. Chem. C*, 2010, **114**, 6849-6853.
53. H.-L. Yip and A. K.-Y. Jen, *Energy Environ. Sci.*, 2012, **5**, 5994-6011.

Table of Contents

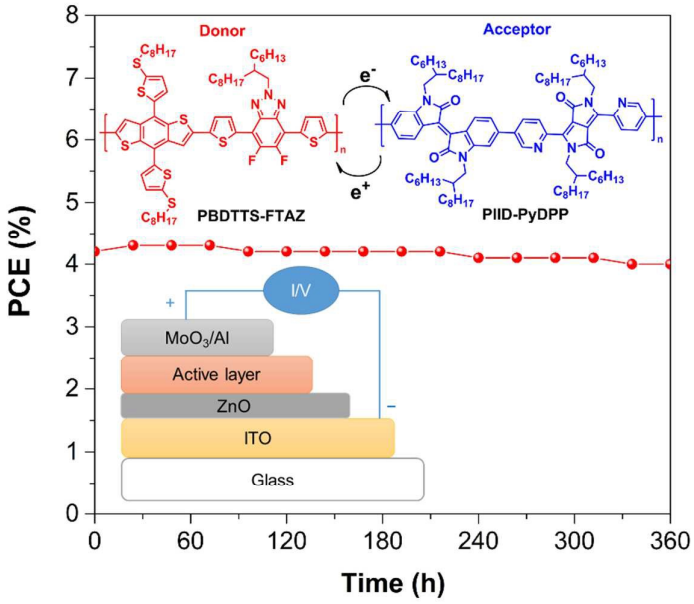

High photovoltage all-PSCs with good stability were realized by using a new polymer acceptor based on diketopyrrolopyrrole-isoindigo.